DETAILED ANALYSIS OF FINE LINE PRINTED AND PLATED SOLAR CELL CONTACTS

D. Pysch, A. Mette*, A. Filipovic, S. W. Glunz

Fraunhofer Institute for Solar Energy Systems, Heidenhofstr. 2, D-79110 Freiburg, Germany
Phone: +49-761-4588-5287; Fax: +49-761-4588-9250; email: damian.pysch@ise.fraunhofer.de
* now with Q-Cells AG, Germany

ABSTRACT: This work presents a detailed analysis of the new *two-layer process* to contact industrial solar cells. The seed layer was created by a pad printer and thickened by light-induced plating of silver. These contact structures were investigated microscopically aiming for a better understanding of the observed solar cell results. First we analysed the influence of the geometry of the seed-layer on IV-parameter. Next, the dependence of the contact resistance on the width of the seed-layer was measured and compared with theoretical expectations. This comparison resulted in the conclusion that the contact resistivity decreases with a reduction of the seed layer width. These results have been further approved by an analysis of SEM-pictures of wet chemically etched contacts. Contact resistance (R_C) measurements before and after light-induced plating of silver showed surprisingly a positive influence of the plating process on R_C. A detailed microscopical analysis revealed four new possible current flow paths due to the light-induced plating of a conventional contact or a seed layer. The results led to an extension of the existing model for a screen-printed contact.
Keywords: silicon solar cells, characterization, contact resistance, two-layer contacts

1 INTRODUCTION

In pursuing the aim of increasing the efficiency η of industrial solar cells to further enhance the productivity, four requirements on the front side grid offer improvement potential: (i) lower the finger-line resistance and (ii) width, (iii) raise the aspect ratio and most important (iv) to reduce the contact resistivity on lowly doped emitters.

The concept of a *two-layer-process* is very promising in managing the above mentioned challenges of contact formation for industrial solar cells [1]. The contact formation process is created by a deposition of a thin *seed layer* for the actual contact formation which is then enhanced by a *growth* plating step [2]. The main advantage of the *two- layer-process* is that each layer can be optimized and analysed individually. The seed layer should exhibit a low contact resistivity to the underlying emitter layer and a low contact width. The second (plating) layer should guarantee a low finger-line resistance. Currently, we are investigating four different methods to deposit a fine line seed layer at Fraunhofer ISE [3, 4].

Previous investigations have shown that the contact resistivity rises with decreasing the finger line width. Furthermore, we observed evidence for a positive influence of the plated layer on the contact resistance.

In this paper the influence of the seed layer height and width on the contact resistance is investigated. The seed layer was created using a pad printer and hotmelt ink [5]. Hence, the results can be transferred to all screen print particle-based pastes. With our investigations we aim to improve the understanding of the contact formation and the awareness of present problems for fine-line printed contacts. Furthermore, the influence of the plating step on the contact interface is examined.

2 EXPERIMENTAL

The investigations of the sections 3 to 4.1 were carried out on planar Cz-silicon solar cells with a base resistivity of 1-2 Ω cm, an Al-BSF, a SiN_X-anti reflection coating (ARC), an emitter sheet resistance R_{SH} of 55 Ω/sq. and a pad printed hotmelt ink front side grid with a finger width W_{seed} of 70 µm (Fig. 1). The number of print steps was varied from one to four. All wafers were thickened by **l**ight-**i**nduced silver **p**lating (LIP). The microscopical investigations as SEM and AFM in section 4.2 were carried out on cells with the processes described above except for a textured surface and the use of screen printing for seed layer deposition.

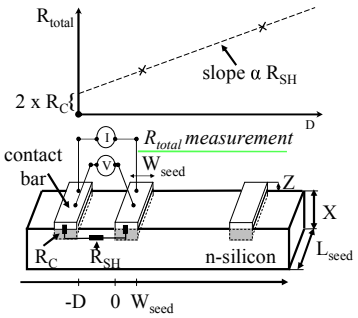


Figure 1: Measurement principle of the used **t**ransmission **l**ine **m**odel TLM-structures to determine the contact resistance and sheet resistance of the emitter by varying the distance D between adjacent contact bars.

The contact resistance was determined using the **t**ransmission **l**ine **m**odel TLM (see Fig. 1) [6]. In this paper we exclusively present the normed contact resistance $R_C L_{seed}$ in order to be independent from the choice of the TLM-structure length L_{seed}. $R_C L_{seed}$ was used instead of the contact resistivity ρ_C for characterisation due to conceptual problems, applying the TLM-theory to determine ρ_C for screen-print paste contacts. For the microscopic investigations we use a **s**canning **e**lectron – (SEM), **a**tomic **f**orce **m**icroscope (AFM), and a **f**ocused **i**on **b**eam (FIB) for cross section preparation.

3 ANALYSIS OF FINE LINE PRINTED CONTACTS

3.1 Solar cell results

Solar cells were pad-printed with a 70 µm seed layer grid. We varied the amount of print steps in order to

HANWHA v. MAXEON
IPR2024-01203
HANWHA 1081

change the seed layer height systematically. The fill factor *FF* and the η are plotted against the number of print steps before and after the plating enhancement (Fig 2). Since the repetition accuracy of the used pad printer was not high, all print steps that followed the initial one, resulted besides the rise of the seed layer height also to a rise of the width. Thus, the shading losses were increased, reducing j_{SC} and η (see Fig. 2).

A conclusion that can be drawn from Figure 2 is that the highest efficiency is achieved through a plated seed layer with a single printing step. The fill factor reaches its maximum after the second print step. The fill factor and consequently the efficiency might be further increased by a longer plating time of the one-print-step solar cells, due to a further reduction of the finger resistance. However, this presumption could not be verified by a second LIP-step (see Fig. 2). The FF rises only marginally ($FF \approx 77.7\%$) and the efficiency stays unchanged. Hence, the contact height after a single pad-print-step ($Z \approx 2$ µm) seems to be insufficient to form a contact resistivity comparable to the two or more-print-step seed layers.

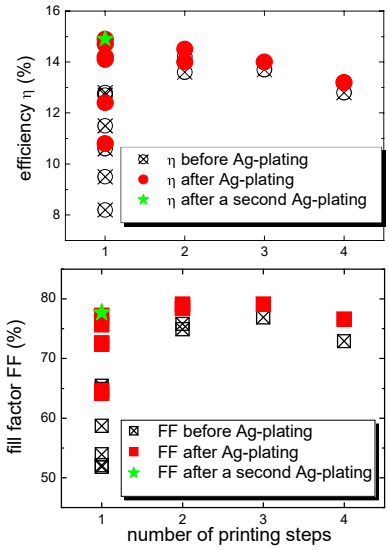


Figure 2: Efficiency η and fill factor *FF* as a function of the number of printing steps repetitions of the seed layer before and after an additional plating growth step of the contact finger by LIP.

3.2 Contact resistance analysis

On the same wafers, five TLM-structures (40-100µm contact width) for contact resistance $R_C L_{seed}$ and sheet resistance R_{SH} measurements were simultaneously pad-printed with the solar cells.

Figure 3 shows the dependance of the contact resistance on the seed layer width W_{seed}. As the single-print-step structures showed the most reliable values, they were used for further investigations. Each point in Figure 3 is a mean value of at least two TLM-measurements. We fitted a calculated graph (see Eq. (1)) to the last to measurement points with approximately constant $R_C L_{seed}$ values, applying the following equation (see solid line in Fig.3):

$$R_C L_{seed} = \left(\sqrt{\frac{\rho_C}{R_{SH}}}\right) R_{SH}\ \mathrm{cotanh}\left(\sqrt{\frac{R_{SH}}{\rho_C}} W_{seed}\right) \qquad (1)$$

By comparing the measurements with the theoretically expected characteristics (solid line in Fig. 3), an increasing deviation with decreasing finger width appears. Hence, we fitted each measured contact resistance value by an individual simulated graph with ρ_C as fit parameter. This procedure results in a contact resistivity value for each seed layer width. The sheet resistance R_{SH} = 53.2 ± 3.0 Ω/sq., which was used for calculation, is a mean value of about 30 measured TLM-structures.

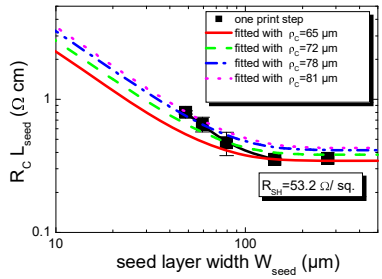


Figure 3: Contact resistance plotted versus the seed layer width. Each measurement point is fitted applying Eq. (1) (with the contact resistivity as fit parameter).

Based on these microscopical results (see Fig 3) it is possible to conclude, that the contact quality drops with decreasing seed layer width, for the used paste under investigation.

3.3 Microscopic examination of the seed layer

To obtain a better understanding of the macroscopic results, we cleaved the TLM-structures perpendicular to the seed layers. At the one half of the cleaved TLM-structures we removed the seed layer wet-chemically. The resulting "fingerprint" on the n-silicon was analysed by a SEM, directly at the breaking edge (Fig. 4 left). The typical shape of the silver crystallites (rectangular imprints of the inverted pyramids) appeared on sites were the SiN_X-ARC was completely removed (Fig. 4 left). The ratio of the area of silicon to SiN_X-ARC and the number of crystallite imprints per area under consideration was determined using computer software (see Fig 4 right). Simultaneously we determined a height profile also directly at the breaking edge of the other TLM-structure half. Thus, we can correlate the measured microscopic indicators, namely the crystallite density and SiN_X-coverage, with the height profile of the seed layer at each position (see Fig. 4 & 5).

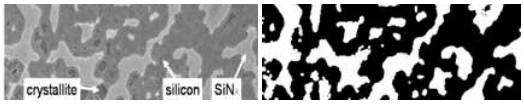


Figure 4: Measurement principle of the used software to analyze the SEM pictures quantitatively. Original SEM-picture (left-hand). Correspondent software-picture of the same section (right hand).

Figure 5 gives a first hint that the etching behaviour of the paste content (the glass frit) depends on the seed

layer height. Six different seed layers were analyzed in the same way as described above, leading to comparable results (e.g. see Figure 5). Out of each of these six graphs three measurement points of each profile were extracted at the middle of the finger and plotted against each other (see Fig. 6). It seems that the crystallite density rises approximately linearly with seed layer height. The SiN_X-coverage-ratio does not show such a clear trend. For the used paste, firing temperature (790°C) and seed layers heights (Z> 4µm), a minimum SiN_X-coverage of just around 40% can be reached.

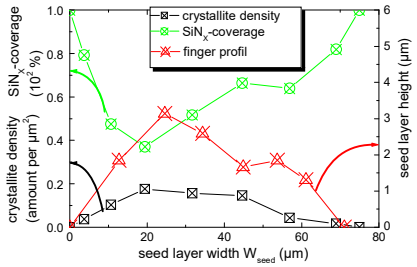


Figure 5: Profiles of the finger height, the crystallite density, and n-Si to SiN_X-coverage ratio of a seed layer.

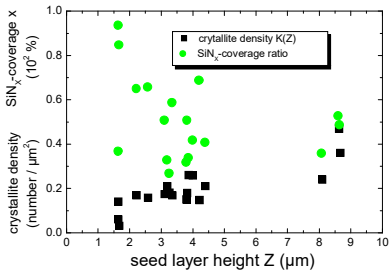


Figure 6: The dependence of the crystallite density and etching ratio of the seed layer height.

To sum up the results of section 3, we can conclude, that the thin seed layer provides a much smaller volume of contacting paste. Hence, there is less glass frit per contact area. This results in a lower etching rate. A minor $SiNB_X$-etching and a lower crystallite density are logical consequences. We believe that this is the reason for the increase in contact resistivity with decreasing seed layer width, assuming that the height decreases simultaneously with the width. We suggest two solutions; either the height of the seed-layer is increased (with maintaining the small width), or to raise the glass frit fraction directly in the contacting paste to get a similar glass amount at the interface compared to screen-printed contacts.

4 INFLUENCE OF AG-PLATING ON THE CONTACT RESISTANCE

4.1 Macroscopic measurements

To investigate a possible influence on the contact resistance through the enhancement of the seed layer by LIP, we measured the contact resistance $R_C L_{seed}$ of the same seed layer before and after plating for eight different TLM-structures (see Fig. 7). A significant trend appears, suggesting a positive influence of the plating on the contact resistance. All $R_C L_{seed}$ values after the plating are smaller than the values before. It seems that plating of silver creates new current paths from the silicon to the contact metal. To verify this assumption we investigated the TLM-structures microscopically using a SEM and AFM.

4.2 Microscopic investigations

In order to find an origin for the observed improvement of the contact resistance due to LIP, the area next to the seed layer was investigated before plating. SEM analysis showed a presumed leakage-film of a width of approximately 5µm (see Fig. 8a). A higher magnification of this layer is shown in Fig 8 b) (marked by a square in Fig. 8 a). The bright areas are assumed to be Ag- and Pb- precipitates and the dark dots to be holes.

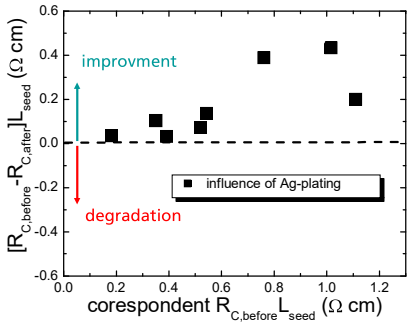


Figure 7: The difference between the contact resistance values is plotted versus the correspondent contact resistance value before LIP of the seed layer. All contacts (good and bad) are electrically improved by LIP.

The identification of the leakage-film with a leaked glass frit film is very likely. The just mentioned presumptions regarding the identification of the leakage-film as a glass frit leakage film could be verified by cross-section SEM-pictures (see Fig. 9a & 12). In figure 9 a) one can identify crystallites under the seed layer as well as in the glass frit leakage film.

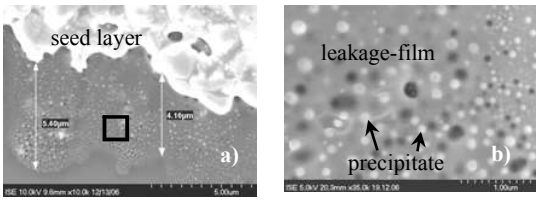


Figure 8: SEM-pictures of the area next to the seed layer (a). A presumed seed layer leakage-film with a width of approximatly 5 µm is observed. The SEM-picture (b) shows a higher magnification of the area marked in the picture (a). The bright areas are assumed Ag- or Pb-precipitates, the dark areas holes.

Two processes are able to create such a leakage film: The seed layer shrinks during the firing process due to the sinter process of the Ag-particle and leaves the glass layer behind and/or the glass frit has a low transition temperature and due to this also a low viscosity around the peak firing temperature. Thus, the glass might wet the n-Si surface very well, resulting in a leakage of the glass out of the seed layer.

On a similar probe as in Fig. 9 a) we removed all the seed layer components wet chemically. The resulting "fingerprint" showed a high crystallite imprint density within the area where the SiN_X was almost unaffected.

We assume that this area correlates with the glass frit layer leakage film area (see Fig. 9 b).

In Fig. 8 b) we assumed the black areas as holes in the glass frit. This assumption could be approved by AFM-measurements of the leaked glass frit film (see Fig 10). We determined the height of the glass leakage film around 200-300 nm. The holes seem to be as deep as the glass film high is. The measurement accuracy was limited due to geometry of the AFM-needle.

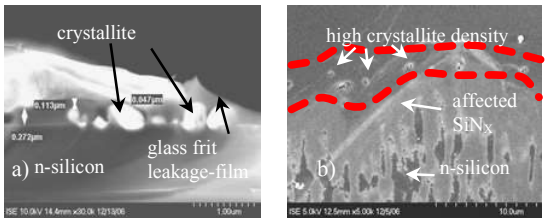


Figure 9: a) Cross-section SEM-picture of the seed layer. The leakage film can be identifed as glass frit. b) Wet chemically etched seed layer, revealing an ambit with a high cristallite density in the area where the glass frit leakage film is assumed to be before etching.

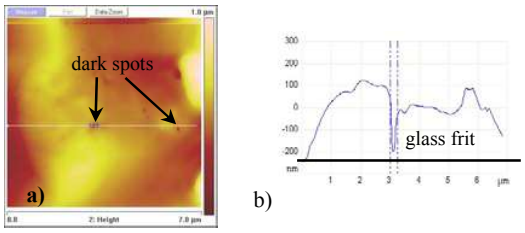


Figure 10: a) AFM-measument of a glass frit leakage film. The graph b) shows the height-profile along the white-line in the AFM-picture (a). Thus, the black spots in the SEM-pictures of Fig. 8 can be identified as holes.

In order to create a perfect cross-section of a two-layer contact finger we prepared a sample using a focused ion beam FIB at the Fraunhofer Institute for Mechanics of Materials IWM in Halle and took SEM pictures of the cross-section (see Fig. 11).

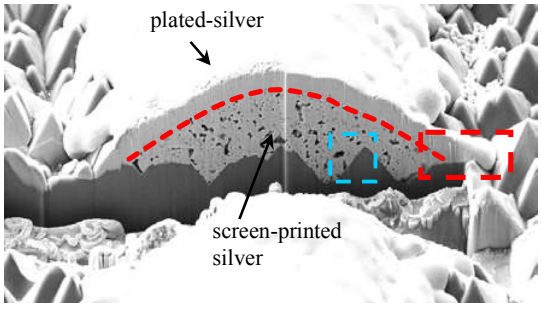


Figure 11: SEM-picture of a cross-section of a two layer contact prepared by FIB machining. One can distinguish very well the dense plated silver from the porous screen-printed one. The marked areas (squares) are shown in a higher magnification in Fig. 12 &13.

The LIP-layer has over the whole contact an almost constant squares thickness. However, it is obvious that on the right end the height almost doubles (see Fig 11 dotted square). Figure 12 shows this area in higher magnification. Three conclusions can be deduced based on this SEM-picture: (i) again we can identify a glass frit leakage-film. (ii) There seems to be a good electrical contact between the glass frit leakage-film and the LIP-silver, since there is a very tight connection. We assume that the plated silver has also grown on top of the glass frit leakage-film, creating an obviously good connection. (iii) The effective contact area is much higher under the LIP-silver than under the screen-printed seed layer silver, due to a more even contact area.

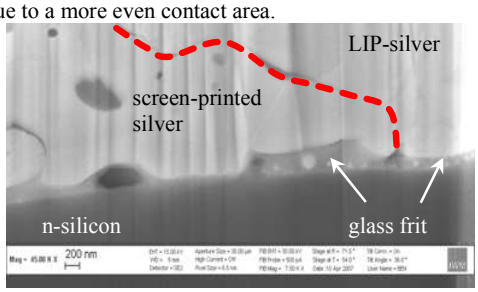


Figure 12: SEM-picture of a cross-section prepared by a FIB. This picture shows a higher magnification of the doted square maked in Figure 11. A glass frit leakage-film can be observed and a very good connection (mechanical and electical) seem to exist between the leakage film and the LIP-silver.

Another nice result is that we could determine the height of the isolating glass frit to a value less than 30 nm (see Fig 13 circle). Likely, the glass frit height might be even thinner at some locations. Thus, it is probable that a quantum mechanical current could pass the extremely thin glass layer at this position. This position correlates very well with the assumed 2nd current path of the existing microscopical model for screen-printed contacts (see Fig. 14).

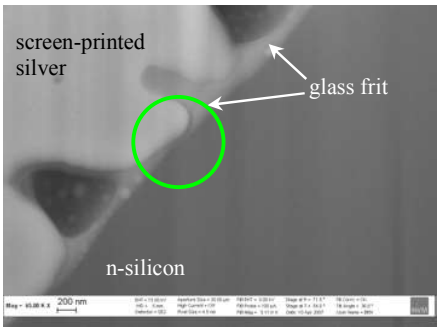


Figure 13: SEM-picture of a cross-section prepared by a FIB. This picture shows a higher magnification of the solid square marked in Figure 11. There are sites observable where the height of the glass frit shrinks below approximatly 30 nm (circle).

In conclusion, in our opinion it is theoretically possible to create a low contact resistivity using silver, but only in absence of glass frit. However, the glass frit is needed to form contacts with good adhesion and to penetrate the isolating SiN_X-layer. Thus, a well balanced

amount of glass frit with the proper etching properties is crucial for a low contact resistivity.

5 MICROSCOPIC CONTACT MODEL

5.1 Existing microscopic model for screen-printed contacts

Within the last years, the understanding of the contact formation process of screen-printed contacts has been extensively improved [7-10]. In the following we give a brief review of the present microscopic model for screen-printed contacts. A typical screen printing paste consists of organic components, solvents, silver-particles and a glass frit (typically lead borosilicate glass). The organic components and the solvents are burned out completely in a temperature-plateau (T≈400°C). A further increase of temperature (T>550°C) is leading to a continuous melting of the glass frit. Furthermore the Ag-particles begin to sinter together forming a sponge-like structure. The liquid glass frit wets the interface between the SiN_X and the sintered bulk-silver. At temperatures exceeding 700°C the glass frit starts to etch the SiN_X-layer locally. At places were the SiN_X-layer is completely removed, the glass also begins to etch the n-Si emitter anisotropically, resulting in inverted pyramids on plane [100]-wafer. In the cooling down phase, silver recrystallizes along the {111}-planes of the inverted pyramids forming a very low contact resistivity at this position [11, 12]. The final state of a screen-printed contact at room temperature is illustrated in Fig. 14. A very nice investigation was presented by Schubert [12], in which he analyses the chemical and physical mechanisms which lead to the above described observations during the contact formation processes.

In Figure 14 three possible current paths are shown: 1st a direct connection between the Ag-crystallite and the bulk-silver. This is desirable situation, due to a very low contact resistivity. 2nd a tunnel current via a very thin (isolating) glass layer and, 3rd a multi tunnel current via the isolating glass and small Ag and Pb precipitates [9]. It is generally accepted that a thick glass layer leads to a local isolating position of the contact (see Fig .14 (4th)).

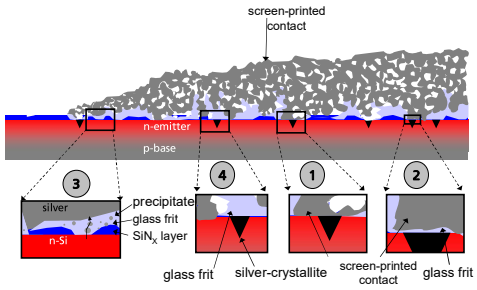


Figure 14: Sketch of the existing contactformation modell of screen-printed solar cell contacts. Three possible scenarios of a currentflow through the contact (1-3) and one isolating contact position (4) are illustrated.

5.2 Extension of the contact model for screen-printed and plated contacts

Based on the results of section 4 we propose an extension in possible current flow paths of the existing contact-model for solely screen-printed solar cell contacts in the presents of an additional plated silver layer. The four new current paths are: 1st) a multi tunnel current via the isolating glass and small Ag and Pb precipitates towards the plated-silver (see (4) in Fig 15). We assume that this current path creates a very good connection between the glass frit leakage-film and the LIP-silver (see Fig 12). 2nd) a current flow might also be possible, if a hole in the glass frit leakage-film is filled with LIP-silver, creating a direct connection to the emitter (see (5) in Fig 15). 3rd) we assume an even higher current flow, if the plated-silver connects directly a crystallite (see (6) in Fig 15). 4th) we can not exclude that the LIP-silver can fill up voids at the edge of the seed layer, creating in the optimum situation a direct contact to a crystallite.

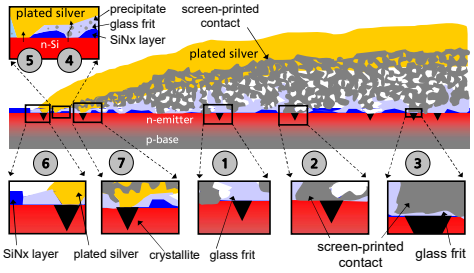


Figure 15: Sketch of the extended contactformation modell of screen-printed and plated solar cell contacts. Four new possible scenarios of a current flow through the contact (4-7) are illustrated.

7 CONCLUSIONS

We used a pad printer to create the seed layer for a two-layer contact-system. A single print step seed layer showed the best solar cell results due to the smallest shading losses. Based on the results of a comparison of measured contact resistance values and their dependence on the seed layer width to theoretically expected graphs, it was possible to conclude that the contact quality drops with decreasing seed layer width. This result could be further verified by a systematic analysis of SEM-pictures. It seems that the crystallite density rises approximately linear with seed layer height. The SiN_X-coverage-ratio does not show such a clear trend. All this observation led to a proposal, how a conventional screen printing paste should be modified in using it as a fine line seed layer.

Contact resistance measurements revealed a positive influence of the LIP-silver on the contact resistance. Microscopical investigations approved the presence of a glass frit leakage-film. For plated seed layers or screen-printed contacts we proposed an extension of the existing contact-model illustrating new current paths.

ACKNOWLEDGEMENTS

The authors would like to thank A. Leimenstoll, and A. Herbolzheimer for cell processing as well as D. Hertkorn and E. Schäffer for support in TLM- and solar cell measurements. This work has been supported by the German Federal Ministry for the Environment, Nature Conservation and Nuclear Safety (BMU) under contract no. 0329960 and 0327569A. We also like to thank the colleagues from Fraunhofer IWM in Halle for preparing the FIB-samples.

REFERENCES

[1] S.W. Glunz, A. Mette, M. Alemán, P.L. Richter, A. Filipovic and G. Willeke, Proceedings of the 21st European Photovoltaic Solar Energy Conference, Dresden, Germany (2006) 746.
[2] A. Mette, C. Schetter, D. Wissen, S. Lust, S.W. Glunz and G. Willeke, Proceedings of the 4th World Conference on Photovoltaic Energy Conversion, Waikoloa, Hawaii, USA (2006) 1056.
[3] M. Alemán, A. Streek, P. Regenfuß, A. Mette, R. Ebert, H. Exner, S.W. Glunz and G. Willeke, Proceedings of the 21st European Photovoltaic Solar Energy Conference, Dresden, Germany (2006) 705.
[4] M. Hoerteis, et al., this conference..
[5] D.M. Huljic, S. Thormann, R. Preu, R. Lüdemann and G. Willeke, Proc. 29th IEEE PVSC, New Orleans, Louisiana, USA (2002) 126.
[6] D.K. Schroder and D.L. Meier, IEEE Transactions on Electron Devices ED-31 (1984) 637.
[7] C. Ballif, D.M. Huljic, G. Willeke and A. Hessler-Wyser, Applied Physics Letters 82 (2003) 1878.
[8] D. Huljic. Fraunhofer ISE und Universität Konstanz, Freiburg / Konstanz 2003.
[9] M.M. Hilali, B. To and A. Rohatgi, Proceedings of the 14th Workshop on Crystalline Silicon Solar Cells and Modules NREL, Winter Park, Colorado, USA (2004) 109.
[10] G. Schubert, F. Huster and P. Fath, Proceedings of the 19th European Photovoltaic Solar Energy Conference, Paris, France (2004) 813.
[11] D.M. Huljic, C. Ballif, A. Hessler-Wyser and G. Willeke, Proceedings of the 3rd World Conference on Photovoltaic Energy Conversion, Osaka, Japan (2003) 83.
[12] G. Schubert. Dissertation, Universität Konstanz, Konstanz 2006.